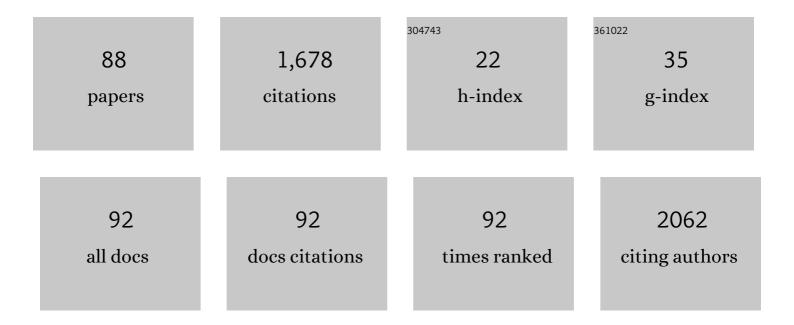
Cornelia Rodenburg

List of Publications by Year in descending order

Source: https://exaly.com/author-pdf/6984258/publications.pdf

Version: 2024-02-01



#	Article	IF	CITATIONS
1	Interfacial Morphology between Ramie Fibers and Phenolic Resins: Effects of Plasma Treatment and Cure Cycle. Journal of Composite Materials, 2022, 56, 889-897.	2.4	4
2	Low-voltage SEM of air-sensitive powders: From sample preparation to micro/nano analysis with secondary electron hyperspectral imaging. Micron, 2022, 156, 103234.	2.2	13
3	Identifying and mapping chemical bonding within phenolic resin using secondary electron hyperspectral imaging. Polymer Chemistry, 2021, 12, 177-182.	3.9	10
4	Controlling Pbl ₂ Stoichiometry during Synthesis to Improve the Performance of Perovskite Photovoltaics. Chemistry of Materials, 2021, 33, 554-566.	6.7	13
5	Spinning Beta Silks Requires Both pH Activation and Extensional Stress. Advanced Functional Materials, 2021, 31, 2103295.	14.9	22
6	Monitoring Carbon in Electron and Ion Beam Deposition within FIB-SEM. Materials, 2021, 14, 3034.	2.9	18
7	Mesoscale structure development reveals when a silkworm silk is spun. Nature Communications, 2021, 12, 3711.	12.8	17
8	Understanding Surface Modifications Induced via Argon Plasma Treatment through Secondary Electron Hyperspectral Imaging. Advanced Science, 2021, 8, 2003762.	11.2	16
9	A novel characterisation approach to reveal the mechano–chemical effects of oxidation and dynamic distension on polypropylene surgical mesh. RSC Advances, 2021, 11, 34710-34723.	3.6	10
10	HelixJet: An innovative plasma source for nextâ€generation additive manufacturing (3D printing). Plasma Processes and Polymers, 2020, 17, 1900099.	3.0	6
11	An Accurate Device for Apparent Emissivity Characterization in Controlled Atmospheric Conditions Up To 1423 K. IEEE Transactions on Instrumentation and Measurement, 2020, 69, 4210-4221.	4.7	7
12	Characterizing Crossâ€Linking Within Polymeric Biomaterials in the SEM by Secondary Electron Hyperspectral Imaging. Macromolecular Rapid Communications, 2020, 41, e1900484.	3.9	10
13	Tensegrity Modelling and the High Toughness of Spider Dragline Silk. Nanomaterials, 2020, 10, 1510.	4.1	11
14	Solvent vapour annealing of methylammonium lead halide perovskite: what's the catch?. Journal of Materials Chemistry A, 2020, 8, 10943-10956.	10.3	11
15	Optimizing size and distribution of voids in phenolic resins through the choice of catalyst types. Journal of Applied Polymer Science, 2019, 136, 48249.	2.6	10
16	Making Sense of Complex Carbon and Metal/Carbon Systems by Secondary Electron Hyperspectral Imaging. Advanced Science, 2019, 6, 1900719.	11.2	14
17	Novel plasma treatment for preparation of laser sintered nanocomposite parts. Additive Manufacturing, 2019, 25, 297-306.	3.0	7
18	Exploiting Plasma Exposed, Natural Surface Nanostructures in Ramie Fibers for Polymer Composite Applications. Materials, 2019, 12, 1631.	2.9	17

CORNELIA RODENBURG

#	Article	IF	CITATIONS
19	Revealing Spider Silk's 3D Nanostructure Through Low Temperature Plasma Etching and Advanced Low-Voltage SEM. Frontiers in Materials, 2019, 5, .	2.4	9
20	Mapping Polymer Molecular Order in the SEM with Secondary Electron Hyperspectral Imaging. Advanced Science, 2019, 6, 1801752.	11.2	19
21	Anisotropic Approach for Simulating Electron Transport in Layered Materials: Computational and Experimental Study of Highly Oriented Pyrolitic Graphite. Journal of Physical Chemistry C, 2018, 122, 10159-10166.	3.1	14
22	Dark electrical bias effects on moisture-induced degradation in inverted lead halide perovskite solar cells measured by using advanced chemical probes. Sustainable Energy and Fuels, 2018, 2, 905-914.	4.9	32
23	New perspectives on nano-engineering by secondary electron spectroscopy in the helium ion and scanning electron microscope. MRS Communications, 2018, 8, 226-240.	1.8	23
24	Searching for order in atmospheric pressure plasma jets. Plasma Physics and Controlled Fusion, 2018, 60, 014038.	2.1	15
25	"Secondary electron spectra of semi-crystalline polymers – A novel polymer characterisation tool?â€ . Journal of Electron Spectroscopy and Related Phenomena, 2018, 222, 95-105.	1.7	9
26	Localized effect of PbI ₂ excess in perovskite solarÂcells probed by high-resolution chemical–optoelectronic mapping. Journal of Materials Chemistry A, 2018, 6, 23010-23018.	10.3	47
27	Stoichiometry-dependent local instability in MAPbI ₃ perovskite materials and devices. Journal of Materials Chemistry A, 2018, 6, 23578-23586.	10.3	21
28	High-Efficiency Spray-Coated Perovskite Solar Cells Utilizing Vacuum-Assisted Solution Processing. ACS Applied Materials & Interfaces, 2018, 10, 39428-39434.	8.0	74
29	Highâ€Performance Multilayer Encapsulation for Perovskite Photovoltaics. Advanced Energy Materials, 2018, 8, 1801234.	19.5	68
30	Surface modification of the laser sintering standard powder polyamide 12 by plasma treatments. Plasma Processes and Polymers, 2018, 15, 1800032.	3.0	9
31	Optimized organometal halide perovskite solar cell fabrication through control of nanoparticle crystal patterning. Journal of Materials Chemistry C, 2017, 5, 2352-2359.	5.5	12
32	Nanoscale Mapping of Bromide Segregation on the Cross Sections of Complex Hybrid Perovskite Photovoltaic Films Using Secondary Electron Hyperspectral Imaging in a Scanning Electron Microscope. ACS Omega, 2017, 2, 2126-2133.	3.5	16
33	Mapping Nanostructural Variations in Silk by Secondary Electron Hyperspectral Imaging. Advanced Materials, 2017, 29, 1703510.	21.0	20
34	Low-Voltage SEM of Natural Plant Fibers: Microstructure Properties (Surface and Cross-Section) and their Link to the Tensile Properties. Procedia Engineering, 2017, 200, 295-302.	1.2	24
35	Efficient perovskite photovoltaic devices using chemically doped PCDTBT as a hole-transport material. Journal of Materials Chemistry A, 2017, 5, 15714-15723.	10.3	29
36	Nanoclay/Polymer Composite Powders for Use in Laser Sintering Applications: Effects of Nanoclay Plasma Treatment. Jom, 2017, 69, 2278-2285.	1.9	10

#	Article	IF	CITATIONS
37	Novel organic photovoltaic polymer blends: A rapid, 3-dimensional morphology analysis using backscattered electron imaging in the scanning electron microscope. Solar Energy Materials and Solar Cells, 2017, 160, 182-192.	6.2	12
38	Comparative study of image contrast in scanning electron microscope and helium ion microscope. Journal of Microscopy, 2017, 268, 313-320.	1.8	13
39	Feasibility of Plasma Treated Clay in Clay/Polymer Nanocomposites Powders for use Laser Sintering (LS). IOP Conference Series: Materials Science and Engineering, 2017, 195, 012003.	0.6	3
40	Nanoscale Mapping of Semi rystalline Polypropylene. Physica Status Solidi C: Current Topics in Solid State Physics, 2017, 14, 1700153.	0.8	4
41	Quantitative secondary electron imaging for work function extraction at atomic level and layer identification of graphene. Scientific Reports, 2016, 6, 21045.	3.3	26
42	Sub-5 nm graphene nanopore fabrication by nitrogen ion etching induced by a low-energy electron beam. Nanotechnology, 2016, 27, 195302.	2.6	13
43	Angle selective backscattered electron contrast in the low-voltage scanning electron microscope: Simulation and experiment for polymers. Ultramicroscopy, 2016, 171, 126-138.	1.9	12
44	Indium-free multilayer semi-transparent electrodes for polymer solar cells. Solar Energy Materials and Solar Cells, 2016, 144, 600-607.	6.2	18
45	Application of low-voltage backscattered electron imaging to the mapping of organic photovoltaic blend morphologies. Journal of Physics: Conference Series, 2015, 644, 012017.	0.4	2
46	Separating topographical and chemical analysis of nanostructure of polymer composite in low voltage SEM. Journal of Physics: Conference Series, 2015, 644, 012018.	0.4	2
47	Sub-nanometre resolution imaging of polymer–fullerene photovoltaic blends using energy-filtered scanning electron microscopy. Nature Communications, 2015, 6, 6928.	12.8	56
48	The effect of residual palladium catalyst on the performance and stability of PCDTBT:PC70BM organic solar cells. Organic Electronics, 2015, 27, 266-273.	2.6	46
49	Arginine–glycine–aspartic acid functional branched semi-interpenetrating hydrogels. Soft Matter, 2015, 11, 7567-7578.	2.7	8
50	High-efficiency inverted polymer solar cells via dual effects of introducing the high boiling point solvent and the high conductive PEDOT:PSS layer. Organic Electronics, 2014, 15, 2059-2067.	2.6	7
51	Helium ion microscopy based wall thickness and surface roughness analysis of polymer foams obtained from high internal phase emulsion. Ultramicroscopy, 2014, 139, 13-19.	1.9	9
52	Helium ion microscopy and energy selective scanning electron microscopy – two advanced microscopy techniques with complementary applications. Journal of Physics: Conference Series, 2014, 522, 012049.	0.4	2
53	Imaging the Bulk Nanoscale Morphology of Organic Solar Cell Blends Using Helium Ion Microscopy. Nano Letters, 2011, 11, 4275-4281.	9.1	28
54	Surface morphology of silica nanowires at the nanometer scale. Journal of Non-Crystalline Solids, 2011, 357, 3042-3045.	3.1	5

Cornelia Rodenburg

#	Article	IF	CITATIONS
55	Resolution Limits of Secondary Electron Dopant Contrast in Helium Ion and Scanning Electron Microscopy. Microscopy and Microanalysis, 2011, 17, 637-642.	0.4	12
56	Energy Selective Secondary Electron Detection in SEM for the Characterization of Polymers. Microscopy and Microanalysis, 2011, 17, 880-881.	0.4	1
57	Comparison of multilayered nanowire imaging by SEM and Helium Ion Microscopy. Journal of Physics: Conference Series, 2010, 241, 012080.	0.4	Ο
58	Progress towards site-specific dopant profiling in the scanning electron microscope. Journal of Physics: Conference Series, 2010, 209, 012068.	0.4	3
59	Energy filtered scanning electron microscopy: applications to characterisation of semiconductors. Journal of Physics: Conference Series, 2010, 241, 012074.	0.4	4
60	Energy selective scanning electron microscopy to reduce the effect of contamination layers on scanning electron microscope dopant mapping. Ultramicroscopy, 2010, 110, 1185-1191.	1.9	47
61	The role of helium ion microscopy in the characterisation of complex three-dimensional nanostructures. Ultramicroscopy, 2010, 110, 1178-1184.	1.9	6
62	The effect of oxidation and carbon contamination on SEM dopant contrast. Journal of Physics: Conference Series, 2010, 241, 012078.	0.4	6
63	Energy filtered scanning electron microscopy: Applications to dopant contrast. Journal of Physics: Conference Series, 2010, 209, 012053.	0.4	2
64	Dopant contrast in the Helium Ion Microscope: contrast mechanism. Journal of Physics: Conference Series, 2010, 241, 012076.	0.4	5
65	Quantitative dopant contrast in the helium ion microscope. Europhysics Letters, 2009, 86, 26005.	2.0	15
66	Dopant contrast in the helium ion microscope. Europhysics Letters, 2009, 85, 46001.	2.0	13
67	The Effect of Oxide Overlayers on Secondary Electron Dopant Mapping. Microscopy and Microanalysis, 2009, 15, 237-243.	0.4	17
68	One Year On: New and Unique Applications of He Ion Microscopy. Microscopy and Microanalysis, 2009, 15, 652-653.	0.4	2
69	A comprehensive Monte Carlo calculation of dopant contrast in secondary-electron imaging. Europhysics Letters, 2008, 82, 30006.	2.0	28
70	High resolution dopant profiling in the SEM, image widths and surface band-bending. Journal of Physics: Conference Series, 2008, 126, 012033.	0.4	10
71	A comprehensive Monte Carlo calculation of dopant contrast in secondary-electron imaging. Europhysics Letters, 2008, 82, 49901.	2.0	5
72	A quantitative analysis of the influence of carbides size distributions on wear behaviour of high-speed steel in dry rolling/sliding contact. Acta Materialia, 2007, 55, 2443-2454.	7.9	96

Cornelia Rodenburg

#	Article	IF	CITATIONS
73	Oxidation Behavior and Mechanisms of TiAlN/VN Coatings. Metallurgical and Materials Transactions A: Physical Metallurgy and Materials Science, 2007, 38, 2464-2478.	2.2	26
74	Quantitative secondary electron energy filtering in a scanning electron microscope and its applications. Ultramicroscopy, 2007, 107, 140-150.	1.9	56
75	The influence of beam energy and oxidation on quantitative carbide analysis in the scanning electron microscope. Journal of Applied Physics, 2006, 100, 114902.	2.5	1
76	High resolution quantitative two-dimensional dopant mapping using energy-filtered secondary electron imaging. Journal of Applied Physics, 2006, 100, 054901.	2.5	51
77	Site-specific dopant profiling in a scanning electron microscope using focused ion beam prepared specimens. Applied Physics Letters, 2006, 88, 212110.	3.3	21
78	Mapping the potential within a nanoscale undoped GaAs region using a scanning electron microscope. Applied Physics Letters, 2004, 84, 2109-2111.	3.3	19
79	Effect of experimental parameters on doping contrast of Si p?n junctions in a FEG-SEM. Microelectronic Engineering, 2004, 73-74, 948-953.	2.4	25
80	Hot workability of spray-formed AISI M3:2 high-speed steel. Materials Science & Engineering A: Structural Materials: Properties, Microstructure and Processing, 2004, 386, 420-427.	5.6	31
81	Hot workability of spray-formed AISI M3:2 high-speed steel. Materials Science & Engineering A: Structural Materials: Properties, Microstructure and Processing, 2004, 386, 420-427.	5.6	9
82	Effect of experimental parameters on doping contrast of Si p?n junctions in a FEG-SEM. Microelectronic Engineering, 2004, 73-74, 948-953.	2.4	2
83	Optimizing and quantifying dopant mapping using a scanning electron microscope with a through-the-lens detector. Applied Physics Letters, 2003, 83, 293-295.	3.3	37
84	Investigation of intermixing in TiAlN/VN nanoscale multilayer coatings by energy-filtered TEM. Surface and Coatings Technology, 2002, 151-152, 209-213.	4.8	33
85	Industrial scale manufactured superlattice hard PVD coatings. Surface Engineering, 2001, 17, 15-27.	2.2	117
86	Shortlisted substrate ion etching in combined steered cathodic arc–ubm deposition system: effects on interface architecture, adhesion, and tool performance. Surface Engineering, 2000, 16, 176-180.	2.2	20
87	The interface between TiAlN hard coatings and steel substrates generated by high energetic Cr+ bombardment. Surface and Coatings Technology, 2000, 125, 66-70.	4.8	24
88	Investigation of Perovskite Solar Cells Homogeneity and Defects by Complementary High-Resolution Mapping Techniques. , 0, , .		0